

# A voltage-dependent $\text{Ca}^{2+}$ homeostat operates in the plant vacuolar membrane

Julian Dindas<sup>1,2\*</sup> , Ingo Dreyer<sup>3\*</sup> , Shouguang Huang<sup>1</sup> , Rainer Hedrich<sup>1</sup>  and M. Rob G. Roelfsema<sup>1</sup> 

<sup>1</sup>Molecular Plant Physiology and Biophysics, Julius-von-Sachs Institute for Biosciences, Biocenter, Würzburg University, Würzburg D-97082, Germany; <sup>2</sup>Institute of Plant and Microbial Biology and Zürich-Basel Plant Science Center, University of Zürich, Zollikerstrasse 107, Zürich CH-8008, Switzerland; <sup>3</sup>Center of Bioinformatics, Simulation and Modeling (CBSM), Faculty of Engineering, Universidad de Talca, 2 Norte 685, Talca 3460000, Chile

## Summary

Author for correspondence:

M. Rob G. Roelfsema

Email: roelfsema@botanik.uni-wuerzburg.de

Received: 25 November 2020

Accepted: 5 February 2021

New Phytologist (2021) 230: 1449–1460

doi: 10.1111/nph.17272

**Key words:** *Arabidopsis thaliana*, calcium signalling, computational cell biology, cpYFP cytosolic pH reporter, R-GECO1 cytosolic  $\text{Ca}^{2+}$  reporter, TPC1 channel, vacuolar membrane, voltage clamp.

- Cytosolic calcium signals are evoked by a large variety of biotic and abiotic stimuli and play an important role in cellular and long distance signalling in plants. While the function of the plasma membrane in cytosolic  $\text{Ca}^{2+}$  signalling has been intensively studied, the role of the vacuolar membrane remains elusive.
- A newly developed vacuolar voltage clamp technique was used in combination with live-cell imaging, to study the role of the vacuolar membrane in  $\text{Ca}^{2+}$  and pH homeostasis of bulging root hair cells of *Arabidopsis*.
- Depolarisation of the vacuolar membrane caused a rapid increase in the  $\text{Ca}^{2+}$  concentration and alkalisied the cytosol, while hyperpolarisation led to the opposite responses.
- The relationship between the vacuolar membrane potential, the cytosolic pH and  $\text{Ca}^{2+}$  concentration suggests that a vacuolar  $\text{H}^+/\text{Ca}^{2+}$  exchange mechanism plays a central role in cytosolic  $\text{Ca}^{2+}$  homeostasis. Mathematical modelling further suggests that the voltage-dependent vacuolar  $\text{Ca}^{2+}$  homeostat could contribute to calcium signalling when coupled to a recently discovered  $\text{K}^+$  channel-dependent module for electrical excitability of the vacuolar membrane.

## Introduction

Temporal elevations of the cytosolic free calcium concentration ( $[\text{Ca}^{2+}]_{\text{cyt}}$ ) of plant cells are evoked by a variety of biotic and abiotic stimuli (McAinsh & Pittman, 2009; Roelfsema & Hedrich, 2010). These  $\text{Ca}^{2+}$  spikes can serve as signals within single plant cells, or propagate to enable systemic signalling between distant plant tissues (Choi *et al.*, 2014; Evans *et al.*, 2016; Toyota *et al.*, 2018). Such  $\text{Ca}^{2+}$ -based signals have been implicated in a broad range of functions, including pathogen resistance (Jeworutzki *et al.*, 2010; Ranf *et al.*, 2014; Tian *et al.*, 2019; Thor *et al.*, 2020), defence responses to wounding (Toyota *et al.*, 2018; Marhavy *et al.*, 2019), the signal transduction of hormones (Shih *et al.*, 2015; Dindas *et al.*, 2018; Huang *et al.*, 2019), nutrient sensing (Xu *et al.*, 2006; Tang *et al.*, 2020), as well as adaptive responses to salt stress (Choi *et al.*, 2014; Evans *et al.*, 2016).

In general,  $\text{Ca}^{2+}$  signals can be considered as a transient disturbance of the  $\text{Ca}^{2+}$  homeostasis in plant cells, which controls  $[\text{Ca}^{2+}]_{\text{cyt}}$  at a low resting level of *c.* 100–200 nM (Wheeler & Brownlee, 2008; Roelfsema & Hedrich, 2010; Bose *et al.*, 2011; Tang & Luan, 2017; Kudla *et al.*, 2018). This constant low level is stabilised by a multitude of proteins that bind  $\text{Ca}^{2+}$  and thereby provide a buffer capacity of 0.1–0.5 mM in plant cells

(Trewavas, 1999). In the longer term, low  $[\text{Ca}^{2+}]_{\text{cyt}}$  is maintained by the energy-dependent transport of  $\text{Ca}^{2+}$  ions against their electrochemical gradient across the plasma membrane (PM) and across the intracellular membranes of organelles. So far, four groups of transport proteins have been identified in *Arabidopsis thaliana* that contribute to this process: the autoinhibited  $\text{Ca}^{2+}$ -ATPases (ACAs), ER-type  $\text{Ca}^{2+}$ -ATPases (ECAs), P1-ATPases (as for HMA1) and  $\text{H}^+/\text{Ca}^{2+}$  exchangers (CAX) (Kudla *et al.*, 2018). These  $\text{Ca}^{2+}$  efflux transporters are therefore likely to affect the shape of intracellular  $\text{Ca}^{2+}$  signals but, so far, this has only been shown for the PM-localised efflux transporters ACA8 and ACA10 (Costa *et al.*, 2017; Yang *et al.*, 2017).

$\text{Ca}^{2+}$ -permeable ion channels counteract the active transporters mentioned above and enable a rapid influx of  $\text{Ca}^{2+}$  ions along the steep electrochemical gradient for  $\text{Ca}^{2+}$  across the PM and endomembranes. In recent years, our understanding of the contribution of PM-localised  $\text{Ca}^{2+}$  channels to the generation of cytosolic  $\text{Ca}^{2+}$  signals has expanded considerably. Members of the cyclic nucleotide gated channel (CNGCs), hyperosmolarity-induced  $[\text{Ca}^{2+}]$  channels (OSCA) and glutamate receptor-like channels (GLRs) families were shown to be involved in several physiological processes such as auxin signalling (Shih *et al.*, 2015; Dindas *et al.*, 2018), plant immunity (Yuan *et al.*, 2014; Tian *et al.*, 2019; Thor *et al.*, 2020), reproduction (Frietsch *et al.*, 2007; Michard *et al.*, 2011; Tunc-Ozdemir *et al.*, 2013; Wudick

\*These authors contributed equally to this work.

*et al.*, 2018; Pan *et al.*, 2019) and long distance systemic signalling (Nguyen *et al.*, 2018; Toyota *et al.*, 2018). In addition, several classes of mechanically activated  $\text{Ca}^{2+}$ -permeable PM channels in plants are likely to be encoded by the *mid1*-complementing activity (MCAs), piezos and MSL1 channels (Kurusu *et al.*, 2013; Hou *et al.*, 2014; Hamilton *et al.*, 2015; Li *et al.*, 2020; Mousavi *et al.*, 2020; Radin *et al.*, 2020).

The central vacuole plays an important role in the cytosolic  $\text{Ca}^{2+}$  homeostasis of plant cells (Martinoia *et al.*, 2012). Calcium is stored in vacuoles at low millimolar concentrations, while its concentration in the cytosol is below one micromolar (Miller & Sanders, 1987; Felle, 1988; Bethmann *et al.*, 1995). Because of this steep concentration gradient, opening of  $\text{Ca}^{2+}$  channels in the vacuolar membrane (VM) will cause a rapid increase in the cytosolic  $\text{Ca}^{2+}$  level. However, little information is known about  $\text{Ca}^{2+}$  channels in the VM. The two-pore channel 1 (TPC1) was initially proposed to act as a  $\text{Ca}^{2+}$ -release channel (Peiter *et al.*, 2005), but it is controversially discussed if this channel is able to conduct  $\text{Ca}^{2+}$  currents under physiological conditions (Hedrich *et al.*, 2018). A recent publication suggested that the voltage-dependent TPC1 channel provides excitability to the VM (Jaslan *et al.*, 2019) by a mechanism in which TPC1 acts in concert with the  $\text{Ca}^{2+}$ -activated  $\text{K}^+$  channels TPK1 and TPK3 (Isayenkov *et al.*, 2010; Jaslan *et al.*, 2019). However, it is still unknown how the apparent excitability of the VM is related to long distance  $\text{Ca}^{2+}$  signalling in plant cells.

To elucidate the role of the VM in  $\text{Ca}^{2+}$  homeostasis, we used a recently developed approach to clamp the VM potential in root hair cells, while simultaneously recording changes in the cytosolic  $\text{Ca}^{2+}$  level and pH (Wang *et al.*, 2015). Our data suggest that the VM acts as a voltage-dependent  $\text{Ca}^{2+}$  homeostat, as a depolarisation of the VM causes an increase in the cytosolic  $\text{Ca}^{2+}$  concentration, while hyperpolarisation provokes the opposite response. It is likely that the voltage pulses affect  $\text{H}^+$ -coupled transport, as depolarising pulses alkalinised the cytosol, while it became more acidic during hyperpolarisation of the VM. Based on these data and the linear relationship between  $\text{Ca}^{2+}$  flux and voltage, we concluded that a vacuolar  $\text{H}^+/\text{Ca}^{2+}$  exchange mechanism plays a central role in cytosolic  $\text{Ca}^{2+}$  homeostasis. In a mathematical modelling approach the vacuolar  $\text{Ca}^{2+}$  homeostat is combined with a recently uncovered module for electrical excitability of the VM (Jaslan *et al.*, 2019), generating a new hypothesis for the link between electrical and  $\text{Ca}^{2+}$  signals.

## Materials and Methods

### Plant material and growth conditions

*Arabidopsis thaliana* seeds were sterilised in 6% NaOCl with 0.05% Triton X-100 and washed with sterile deionised water. Single seeds were subsequently placed on the surface of 1 ml of growth medium (0.12% Murashige & Skoog basal salt mixture including MES, Duchefa; 0.5% sucrose; 1% agarose, pH5.8 with Tris) filled in small Petri dishes ( $\text{\O}$  35 mm). Sealed Petri dishes were placed in a vertically position in a growth chamber (KBWF 720; Binder, Tuttingen, Germany) 3–5 d before the experiments. Growth chambers operated on a 12 h : 12 h, day : night cycle

with temperatures cycling between day : night, 21°C : 16°C, and a light intensity of 120  $\mu\text{mol photons m}^{-2} \text{s}^{-1}$ . The R-GECO1 line (Keinath *et al.*, 2015) was provided by Rainer Waadt (University of Tartu), the GFP line, transformed with GFP5 (Siemering *et al.*, 1996) and with the mutation S65T (Heim *et al.*, 1995), was kindly provided by Melanie Krebs (University of Heidelberg) and the cpYFP line (Behera *et al.*, 2018) was a gift from Markus Schwarzländer (University of Münster).

### Electrophysiology

Microelectrodes were prepared from borosilicate glass capillaries ( $\text{\O}_{\text{out}}$  1 mm,  $\text{\O}_{\text{in}}$  0.58 mm, w/filament, Hilgenberg, Germany). Single-barrelled microelectrodes were pulled with a P-2000 horizontal laser puller (Sutter Instruments, Novato, CA, USA). Double-barrelled microelectrodes were prepared by fusing two glass capillaries through successive heating, turning them by 360° and prepulling them using a customised L/M-3P-A vertical puller (List-Medical-Electronic, Darmstadt, Germany), before the final pull was executed on the horizontal laser puller.

Measurements were conducted in bath solution (5 mM  $\text{CaCl}_2$ , 4 mM KCl, 0.25 mM  $\text{MgCl}_2$ , 0.5 mM NaCl, 1 mM HEPES/KOH pH 7) to which seedlings were accustomed overnight. To this purpose, 2 ml of sterile bath solution was applied to each Petri dish and the Petri dishes were subsequently sealed and placed in a vertical position in the growth chamber. Before measurements, seedling-containing Petri dishes were placed horizontally on an upright microscope and the bath solution was replaced by fresh solution with the same composition (Axioskop 2FS; Zeiss AG, Jena, Germany). Microelectrodes were mounted in a holder of a micromanipulator (MM3A-LMP, Kleindiek Nanotechnik, Reutlingen, Germany) that was used to impale bulging root hair cells. The barrels of the microelectrodes were backfilled with 300 mM KCl and connected with Ag/AgCl half-cells to head stages with input resistance of 100 G $\Omega$ , that were linked to a custom-made microelectrode amplifier (Ullclamp 01). A reference electrode, filled with 300 mM KCl and sealed with an agarose plug (2% w/300 mM KCl), was placed in the solution of the Petri dish. The microelectrode amplifier was equipped with a differential amplifier that enabled double-barrelled electrode, voltage clamp experiments. The voltage and current data were filtered with a four-pole low-pass Bessel filter (LPF 202A; Warner Instruments, Holliston, MA, USA) at 200 Hz and sampled at 1 kHz using the PULSE software (v.8.74, HEKA; Lambrecht/Pfalz, Germany) with an LIH-1600 interface (HEKA), or a UBS-6002 interface (NI, Austin, TX, USA) and WINEDR software (Dempster, 1997). The electrophysiological data were analysed offline using MS EXCEL® (Microsoft, Redmond, WA, USA) and ORIGIN PRO 9 software (OriginLab, Northampton, MA, USA). The microelectrodes were impaled in vacuoles and the electrical potential difference  $E_T$  between bath and vacuolar lumen was measured. Thereafter, the cells were clamped to this value, so that the current at the holding potential was close to 0 nA. Cells in which the current changed more than *c.* 0.1 nA during the measurement were discarded, as it is likely that the PM potential of these cells had changed during the experiment.

## Imaging

R-GECO1 was excited with light from a mercury lamp (Leistungselektronik, Jena, Germany) filtered at 562 nm with a Brightline single-bandpass filter (562/40 nm, Semrock, Rochester, NY, USA) and reflected with a 590 nm dichroic mirror (Zeiss). Light emitted by R-GECO1 was filtered at 628 nm with a Brightline single-bandpass filter (628/40 nm; Semrock). The pH-sensitive cpYFP was excited with an LED illumination system (pE-4000; CoolLED, Andover, UK) at 405 nm and 470 nm (Behera *et al.*, 2018). The emission signal was passed through a dichroic mirror with a cut-off wavelength of 499 nm (Zeiss) and a band filter at 520/35 nm. The cytosolic pH was monitored by calculating the ratio of fluorescence signals obtained with excitation at 470 nm (pH sensitive) and at 405 nm (low pH sensitivity). A decrease in this ratio value indicates a drop in the cytosolic pH (Behera *et al.*, 2018). GFP5 (S65T) was excited with light filtered at 472 nm with a Brightline single-bandpass filter (472/30 nm, Semrock, USA) and reflected with a 490 nm dichroic mirror (Zeiss). Light emitted by GFP was filtered at 520 nm with a Brightline single-bandpass filter (520/30 nm, Semrock). The excitation light was focused on the sample through an Achroplan  $\times 40/0.80$  W objective (Zeiss). Filters and dichroic mirrors described above were placed inside a CARV2 confocal imager (Crest Optics, Rome, Italy) with the spinning disc out of the light path. Filter selection and image acquisition with a charge multiplying CCD camera (QuantEM 512SC; Photometrics, Tucson, AZ, USA) were controlled with Visiview software (Visitron, Puchheim, Germany). For analysis of imaging data, the freeware tool IMAGEJ ([imagej.nih.gov/ij/](http://imagej.nih.gov/ij/)) was used (Schindelin *et al.*, 2012).

## Estimation of the pH-dependent changes in R-GECO1 fluorescence intensity during VM voltages pulses

The fluorescent reporter protein R-GECO1 is sensitive to changes in the cytosolic  $\text{Ca}^{2+}$  concentration, as well as the cytosolic pH (Zhao *et al.*, 2011). As a result, part of the change in R-GECO1 fluorescence intensity, observed during manipulation of the VM potential (Figs 1, 2, 4), could be due to changes in the cytosolic pH. The pH-dependent change of R-GECO1, during application of VM voltage pulses, therefore, was estimated by comparison of the R-GECO1 signals with that of cpYFP, which is highly sensitive to the cytosolic pH (Schwarzländer *et al.*, 2011).

Roots of 6-d-old *A. thaliana* seedlings, which expressed either cpYFP (Supporting Information Fig. S1a), or R-GECO1 (Fig. S1b), were exposed to bath solutions with 50 mM  $\text{CH}_3\text{COONH}_4$ , in which the pH was buffered to pH 6.0 and 6.5 with 2-(N-morpholino)ethanesulfonic acid (MES) and Bis-Tris propane (BTP) and to pH 7.0, 7.5 and 8.0 with BTP and 4-(2-hydroxyethyl)-1-piperazineethanesulfonic acid (HEPES) (Behera *et al.*, 2018). The buffer solutions were exchanged at a speed of  $2.5 \text{ ml min}^{-1}$ , while the volume of the bath was *c.* 1.5 ml.

An LED illumination system (pE-4000; CoolLED, Andover, UK) was used to excite cpYFP at wavelengths of 405 nm and 470

nm and R-GECO1 at 580 nm. The filter wheels in a spinning disc unit (CARV2; Crest Optics, Italy) served to pass the emission signal of cpYFP through a dichroic mirror with cut-off wavelength of 499 nm (Zeiss) and a band pass filter of 520/35 nm, while the R-GECO1 signal was passed through a 590 nm dichroic mirror (Zeiss) and a single-bandpass filter (628/40 nm; Semrock).

The relationship between the extracellular pH and the cpYFP signal, as well as that of the extracellular pH and R-GECO1, could be described with single exponential functions (Fig. S1c, d). Both relationships between extracellular pH and fluorescent reporters were used to obtain an association between cpYFP and the pH-dependent changes in the R-GECO1 signal intensity (Fig. S1e). Based on this association and the changes in cpYFP ratio during voltage pulses ( $470_{\text{ex}}/405_{\text{ex}}$ , Fig. 3b,c), the expected pH-dependent changes in the R-GECO1 signal were calculated and plotted in Fig. 4b,c (grey curves).

## Simulation of thermodynamically ideal transporters

Calculations of the ideal thermodynamic behaviour of transporters were made using the following equations:

### $\text{Ca}^{2+}$ permeable ion channel

$$\Delta G = RT \cdot \log_e \left( \frac{[\text{Ca}^{2+}]_{\text{lum}}}{[\text{Ca}^{2+}]_{\text{cyt}}} \right) - z_{\text{Ca}^{2+}} \cdot F \cdot E_{\text{VM}} \quad \text{Eqn 1}$$

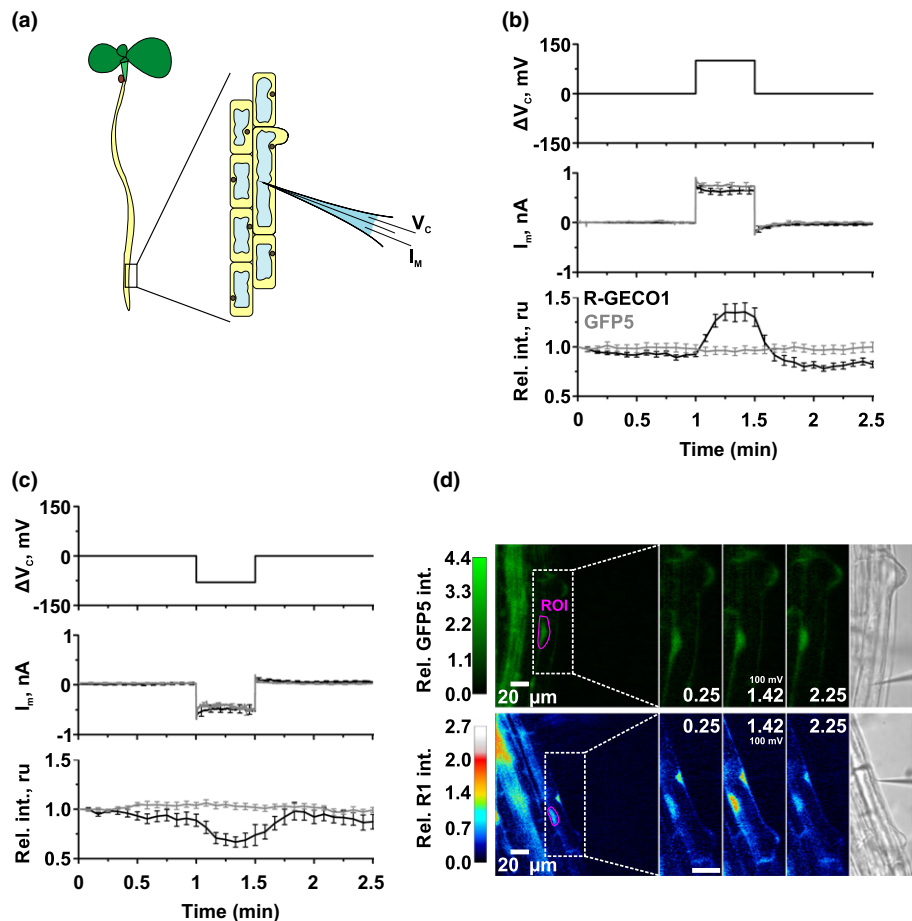
### $\text{H}^+/\text{Ca}^{2+}$ exchanger

$$\Delta G = n_{\text{Ca}^{2+}} \cdot \left[ RT \cdot \log_e \left( \frac{[\text{Ca}^{2+}]_{\text{lum}}}{[\text{Ca}^{2+}]_{\text{cyt}}} \right) - z_{\text{Ca}^{2+}} \cdot F \cdot E_{\text{VM}} \right] - m_{\text{H}^+} \cdot \left[ RT \cdot \log_e \left( \frac{[\text{H}^+]_{\text{lum}}}{[\text{H}^+]_{\text{cyt}}} \right) - z_{\text{H}^+} \cdot F \cdot E_{\text{VM}} \right] \quad \text{Eqn 2}$$

### $\text{Ca}^{2+}$ -ATPase

$$\Delta G = n_{\text{Ca}^{2+}} \cdot \left[ RT \cdot \log_e \left( \frac{[\text{Ca}^{2+}]_{\text{lum}}}{[\text{Ca}^{2+}]_{\text{cyt}}} \right) - z_{\text{Ca}^{2+}} \cdot F \cdot E_{\text{VM}} \right] - m_{\text{H}^+} \cdot \left[ RT \cdot \log_e \left( \frac{[\text{H}^+]_{\text{lum}}}{[\text{H}^+]_{\text{cyt}}} \right) - z_{\text{H}^+} \cdot F \cdot E_{\text{VM}} \right] + \left[ \Delta G_{0,\text{ATP}} + RT \cdot \log_e \left( \frac{[\text{ADP}]_{\text{cyt}} \cdot [P_i]_{\text{cyt}}}{[\text{ATP}]_{\text{cyt}} \cdot 1 \mu\text{M}} \right) \right] \quad \text{Eqn 3}$$

In all equations,  $R$  is the universal gas constant ( $8.3 \text{ J mol}^{-1} \text{ K}^{-1}$ ).  $T$  is absolute temperature (293 K).  $z$  is the valence of the ion ( $z_{\text{Ca}^{2+}} = 2$  and  $z_{\text{H}^+} = 1$ ),  $F$  the Faraday constant ( $9.6 \times 10^4 \text{ C mol}^{-1}$ ) and  $E_{\text{VM}}$  is the VM voltage. For simulation of a  $\text{H}^+/\text{Ca}^{2+}$  exchanger and a  $\text{Ca}^{2+}$ -ATPase,  $n_{\text{Ca}^{2+}}$  and  $m_{\text{H}^+}$  indicate transport stoichiometry. For the  $\text{Ca}^{2+}$ -ATPase  $\Delta G_{0,\text{ATP}}$  is the



**Fig. 1** Voltage pulses applied to the vacuolar membrane (VM) trigger changes in the cytosolic  $\text{Ca}^{2+}$  concentration. (a) Cartoon of the experimental setup, with a double-barrelled microelectrode impaled into the vacuole of a bulging *Arabidopsis thaliana* root hair cell. (b, c) The VM was stimulated with voltage pulses (top panels) of 100 mV (b), or  $-80$  mV (c), which caused changes in vacuolar currents (middle panels, averaged data). A depolarising pulse evoked an increase in the R-GECO1 signal (b, lower panel), while a hyperpolarisation of VM lowered the R-GECO1 fluorescence intensity (c, lower panel). The voltage pulses did not affect the fluorescence of GFP5 (S65T) (bottom panels). Error bars represent SE,  $n = 7$  (GFP5, grey traces), or  $n = 9$  (R-GECO1, black traces) in (b) and  $n = 6$  in (c). Fluorescence signals are given in units that are relative to the value just before the start of voltage pulse. (d) Representative fluorescence images (four panels on left) and transmitted light image (right panels) of bulging root hair cells, expressing GFP5 (S65T) (upper panels) or R-GECO1 (lower panels). The panels in the middle show magnifications of the left panel, as indicated by the white dashed box. The cells were stimulated with a 100 mV voltage pulse at the VM, as in (b). The region of interest (ROI) are encircled by a magenta line in the left panel. Time points and applied voltage pulses are indicated in the middle panels. Fluorescence intensities are linked to the relative fluorescence intensity by the calibration bars on the left.

standard enthalpy for ATP hydrolysis ( $-3.3 \times 10^4 \text{ J mol}^{-1}$ ). the  $ADP/ATP$  ratio was set to 1 and  $[P]_{\text{cyt}} = 70 \mu\text{M}$  (Pratt *et al.*, 2009).

### Computational cell biology

The electrical behaviour of the TPC1/TPK1/3 module was simulated as described in detail in the supplementary material of Jaslan *et al.* (2019), resulting in the time course of  $E_{\text{VM}}(t)$  in response to an external stimulus. The net  $\text{Ca}^{2+}$  flux was experimentally found to be linearly correlated to changes in  $E_{\text{VM}}$  ( $\Delta V_{\text{C}}$ ; Fig. 4d). At the resting voltage, which is negative of the activation threshold of TPC1, there is no net  $\text{Ca}^{2+}$  flux across the tonoplast. Upon hyperpolarisation, the VM mediates a  $\text{Ca}^{2+}$  flux from the cytosol to the vacuole, while it enables a  $\text{Ca}^{2+}$  influx into the cytosol at depolarising potentials. In our model, we

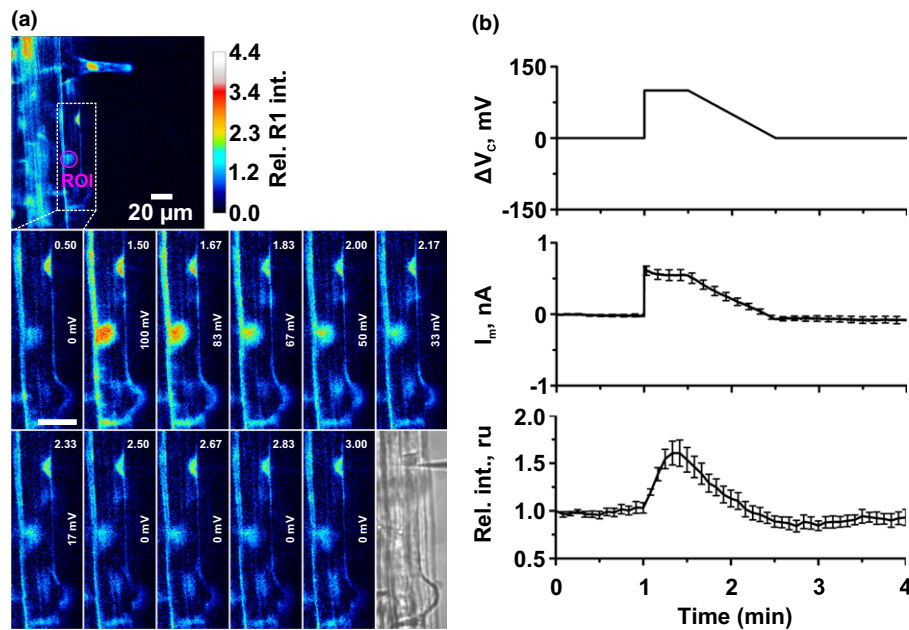
challenged the vacuole with a range of current pulses and determined the changes in  $E_{\text{VM}}$  and  $[\text{Ca}^{2+}]_{\text{cyt}}$  over time. Relative changes in the cytosolic  $\text{Ca}^{2+}$  concentration ( $\Delta[\text{Ca}^{2+}]_{\text{cyt}}$ ) were estimated by integrating the net  $\text{Ca}^{2+}$  flux during tonoplast excitation:

$$\Delta[\text{Ca}^{2+}]_{\text{cyt}} = \alpha \cdot \int (E_{\text{VM}}(t) - E_R) dt \quad \text{Eqn 4}$$

with  $E_R$  being the resting voltage. The unknown proportional factor  $\alpha$  was eliminated by normalisation.

### Results and Discussion

Voltage clamp experiments with guard cells revealed that hyperpolarisation of the PM evokes an increase in  $[\text{Ca}^{2+}]_{\text{cyt}}$  (Grabov &



**Fig. 2** Depolarisation of the vacuolar membrane (VM) increases the cytosolic  $\text{Ca}^{2+}$  concentration. (a) An *Arabidopsis thaliana* root hair cell, of which the VM was stimulated with a voltage ramp. The upper panel shows the R-GECO1 signal of the whole cell, while the lower panels display their magnified images, as indicated by the white dashed box. A magnification of the transmitted light image is shown in the lower right panel. The VM of the cell was stimulated with a depolarising step of 100 mV after 1 min, followed by a gradual return to 0 mV in the following 1.5 min (time indicated in the top of the panels and the voltage at the right side of the panels). The calibration bar (upper right) links the colour code to the fluorescence signal of R-GECO1. (b) Voltage protocol (top panel) used to stimulate the VM of root hair cells, averaged VM currents (middle panels) and averaged relative R-GECO1 fluorescence intensity (bottom panel) at the region of interest (ROI), as shown in upper panel of (a). Error bars show SE ( $n = 7$ ).

Blatt, 1998; Levchenko *et al.*, 2005; Stange *et al.*, 2010; Voss *et al.*, 2016), while long depolarising pulses cause the opposite effect (Stange *et al.*, 2010). The impact of these voltage pulses on  $[\text{Ca}^{2+}]_{\text{cyt}}$  is probably mediated by hyperpolarisation activated cation channels in the PM (Hamilton *et al.*, 2000; Pei *et al.*, 2000; Stoelzle *et al.*, 2003), but so far no genes have been found that encoded these channels. We hypothesised that voltage-activated  $\text{Ca}^{2+}$ -permeable channels may also be active in the VM and therefore tested if voltage pulses applied to the VM also affect  $[\text{Ca}^{2+}]_{\text{cyt}}$ , using the vacuolar voltage clamp approach that was previously described by Wang *et al.* (2015).

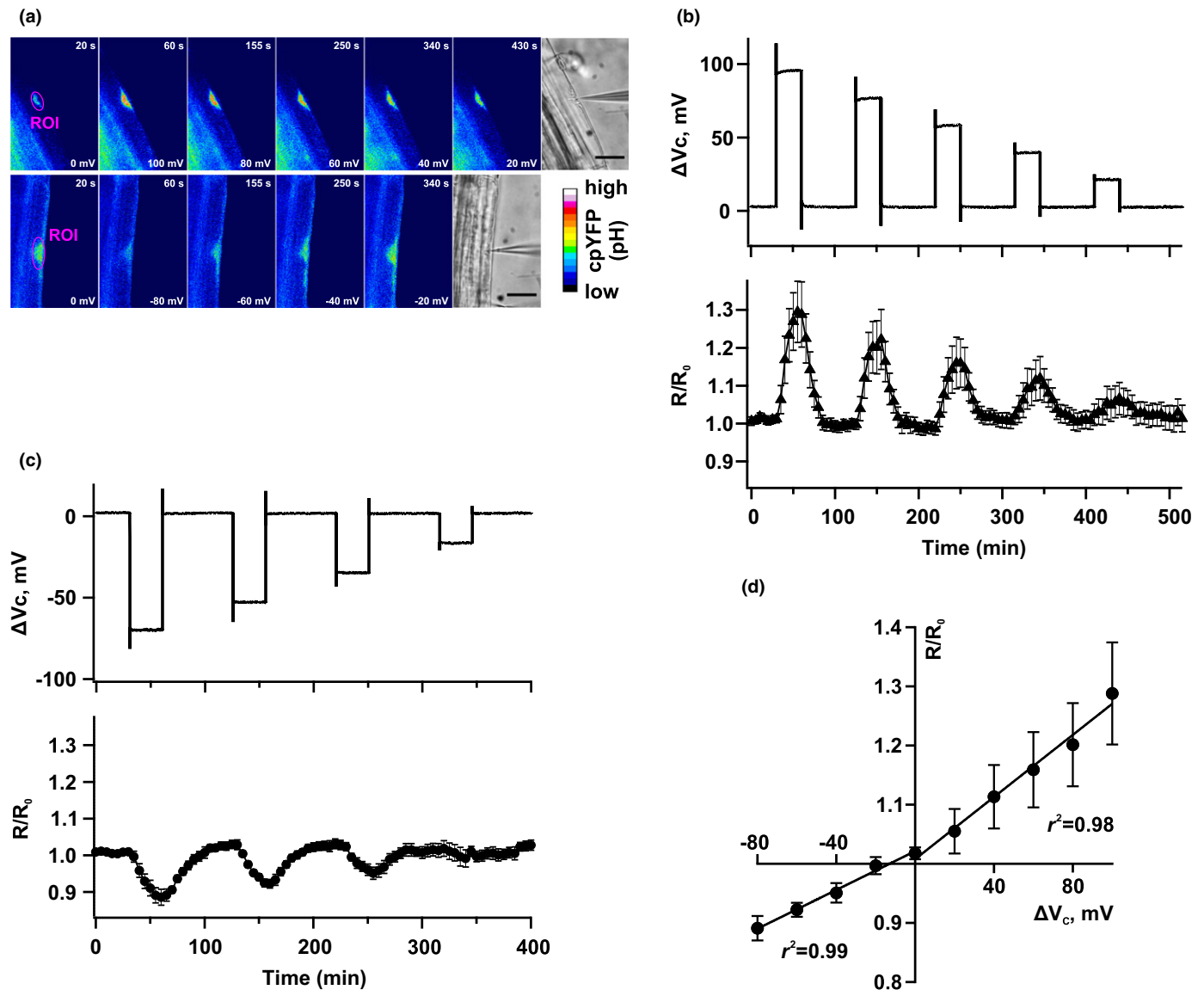
### Voltage stimulation of the VM alters $\text{Ca}^{2+}_{\text{cyt}}$

Double-barrelled microelectrodes were impaled into the body of bulging root hair cells (Fig. 1a), of four 6-d-old *Arabidopsis* seedlings. At this subcellular position, the tip of the electrodes normally penetrates both the plasma and VMs and enables manipulation of the VM potential (Wang *et al.*, 2015). Microelectrodes with vacuolar localisation measured on average an electrical potential difference of 112 mV between bath and vacuolar lumen (standard error (SE) = 2 mV,  $n = 15$ ). According to the convention of membrane voltage measurements on endomembranes (Bertl *et al.*, 1992) the PM and VM potentials should be considered relative to the cytosol and, therefore,  $E_{\text{PM}} = \psi_{\text{cyt}} - \psi_{\text{bath}}$ , while  $E_{\text{VM}} = \psi_{\text{cyt}} - \psi_{\text{vac}}$ . The measured voltage  $E_{\text{T}} = \psi_{\text{bath}} - \psi_{\text{vac}}$  consequently represents  $E_{\text{VM}}$  subtracted by  $E_{\text{PM}}$ ;  $E_{\text{T}} = \psi_{\text{bath}} - \psi_{\text{vac}} = (\psi_{\text{cyt}} - \psi_{\text{vac}}) - (\psi_{\text{cyt}} - \psi_{\text{bath}}) = E_{\text{VM}} - E_{\text{PM}}$ .

Wang *et al.* (2015) found that the VM potential is on average  $-30$  mV, which suggests that the bulging root hair cells had an average PM potential of *c.*  $-142$  mV. After measuring  $E_{\text{T}}$ , the cells were clamped to this value and, therefore, the current at the holding potential was close to 0 nA.

Voltage pulses of 30 s were applied with a  $\Delta V$  of 100 mV, which provoked a depolarisation of the VM from *c.*  $-30$  mV to  $+70$  mV (Fig. 1b, upper panel), while a  $\Delta V$  of  $-80$  mV was applied to hyperpolarise the VM to *c.*  $-110$  mV (Fig. 1c, upper panel). Just as described by Wang *et al.* (2015), such voltage pulses provoked vacuolar currents that slightly decreased during the voltage pulses (Fig. 1b,c, middle panels). On average we determined a VM conductance of 6.5 nS (SE = 0.7 nS,  $n = 9$ ) and 6.1 nS (SE = 1.1 nS,  $n = 6$ ), based on the steady-state currents evoked by depolarising and hyperpolarising pulses, respectively. Under the voltage clamp scenario described, the fluorescence signal of the  $\text{Ca}^{2+}$  reporter R-GECO1 (Zhao *et al.*, 2011; Keinath *et al.*, 2015) was used to monitor changes in  $[\text{Ca}^{2+}]_{\text{cyt}}$  (Fig. 1d).

As a control, a version of GFP5 was used that has a relative low sensitivity to cytosolic pH changes. In a recent study with *Arabidopsis* and tobacco guard cells, it was shown that current injection can lead to osmotically driven cytosolic volume changes (Voss *et al.*, 2016). Due to such volume changes the fluorescence intensity of single-wavelength cytosolic reporters may change and potentially produce false signals. However, we found that pulses of  $\Delta V$  of  $+100$  mV or  $-80$  mV did not affect the GFP5 signal (Fig. 1b,c, lower traces and Fig. 1d, upper panels). Apparently,



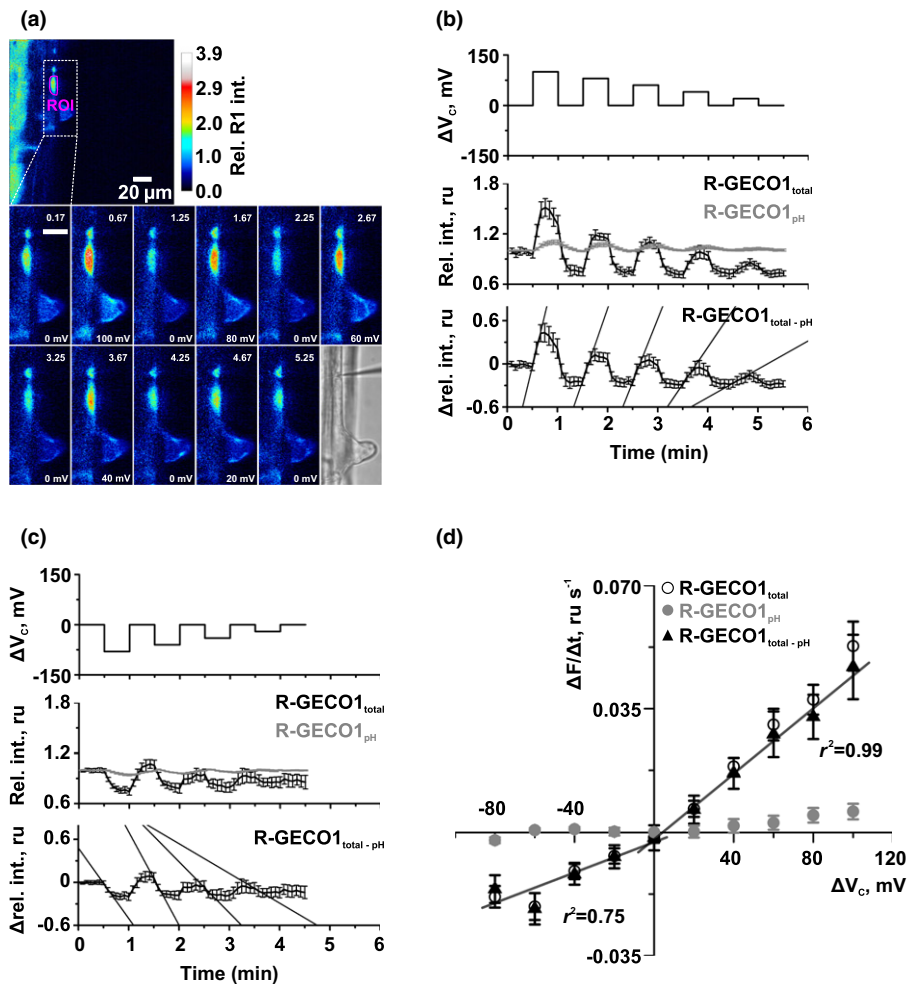
**Fig. 3** A depolarisation of the vacuolar membrane (VM) potential alkalises the cytosol of root hairs. (a) False colour images of the cpYFP ratio ( $470_{ex}/405_{ex}$ ) of *Arabidopsis thaliana* root hair cells, stimulated with depolarising (top row) and hyperpolarising (bottom row) voltage pulses. The time after start of the experiment is indicated in the top of each image and the clamp voltage at the bottom. The panels on the right show the transmitted light images of the same cells. Bar, 20  $\mu\text{m}$ . The calibration bar (lower right panel) links the colour code to the cpYFP fluorescence signal. (b, c) *Top panels*: the VM of root cells was stimulated with depolarising (b, from 100 to 20 mV), and hyperpolarising (c, from -80 to -20 mV) voltage pulses. *Bottom panels*: averaged cpYFP ratio ( $470_{ex}/405_{ex}$ ) of the region of interest (ROI, as shown in left panels of (a)) normalised to the value at the start of the experiment. Error bars show SE ( $n = 9$  in (b) and  $n = 7$  in (c)). (d) Average change of cpYFP ratio ( $470_{ex}/405_{ex}$ ) plotted against the voltage to which VM was clamped. The solid black lines show linear fits of the cpYFP signal with the indicated correlation coefficients. Error bars show SE ( $n = 7-9$ ).

the voltage pulses did not provoke changes in the cytosolic volume of root hairs. By contrast, the depolarising pulses caused a rapid increase in the R-GECO1 signal, while hyperpolarising pulses evoked the opposite response (Fig. 1b,c, lower panels and Fig. 1d, lower panels). This suggests that a depolarisation of the VM causes an influx of  $\text{Ca}^{2+}$  into the cytosol, whereas hyperpolarisation results in an increased  $\text{Ca}^{2+}$  loading of the vacuole.

Voltage pulses applied to the VM in intact root hair cells, also provoked small potential changes in the PM (Wang *et al.*, 2015), which could have induced activation of hyperpolarisation activated  $\text{Ca}^{2+}$ -permeable channels. However, experiments in which

only the PM potential was manipulated showed that these small PM potential changes (on average 8 mV) do not affect  $[\text{Ca}^{2+}]_{\text{cyt}}$  (Fig. S2).

The relationship between the VM potential and  $[\text{Ca}^{2+}]_{\text{cyt}}$  was studied in further detail, by applying a voltage protocol in which  $\Delta V_T$  ( $\psi_{\text{bath}} - \Delta\psi_{\text{vac}}$ ) was first stepped to +100 mV and thereafter changed to 0 mV in a voltage ramp with a rate of  $1.67 \text{ mV s}^{-1}$  (Fig. 2a,b). The R-GECO1 signal showed that  $[\text{Ca}^{2+}]_{\text{cyt}}$  increased after the depolarising voltage step and returned to the original value during the subsequent voltage ramp.



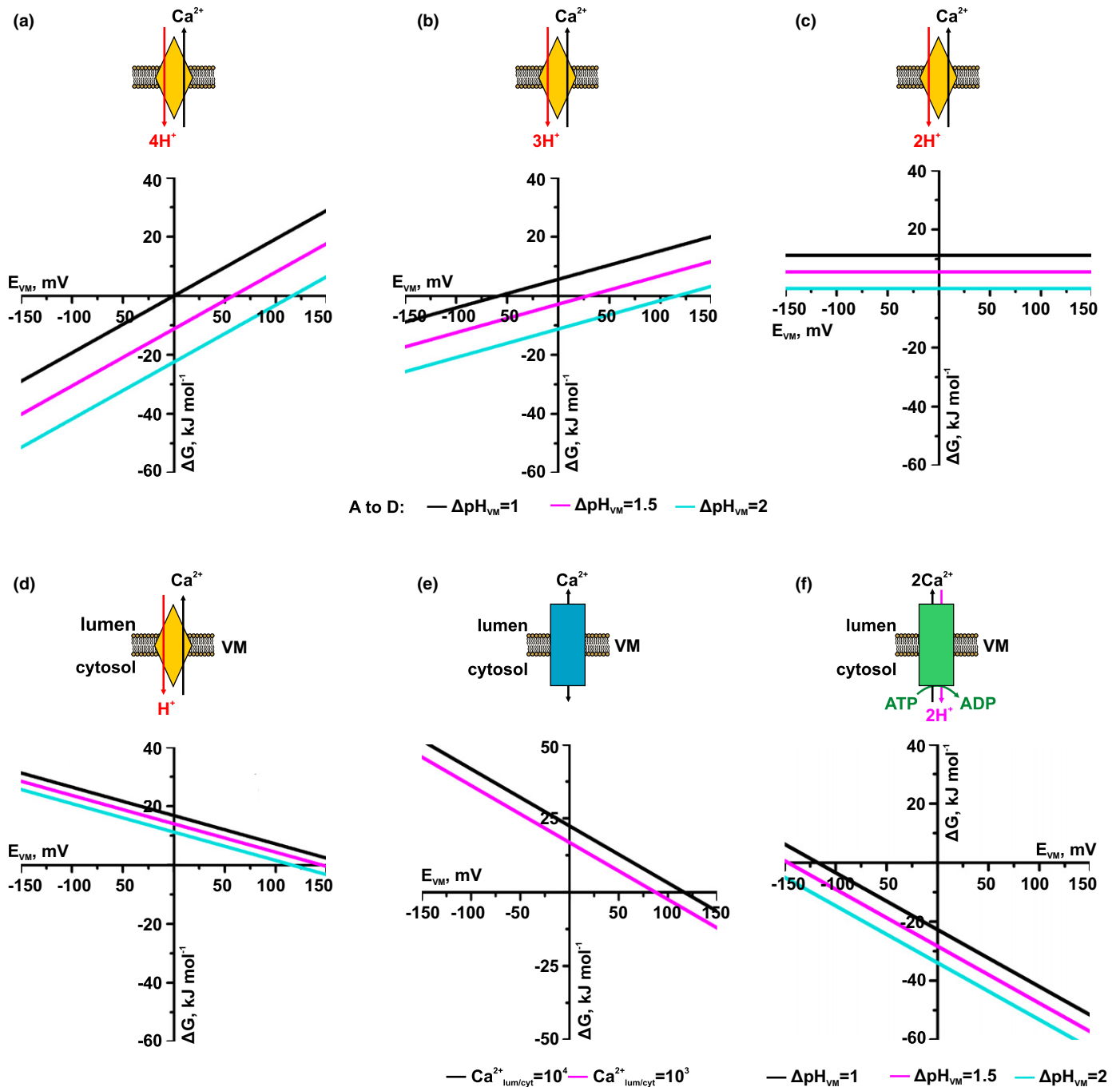
**Fig. 4** The root hair cytosolic  $\text{Ca}^{2+}$  concentration depends on the vacuolar membrane (VM) potential. (a) False colour images of an *Arabidopsis thaliana* root hair cell, of which the VM was stimulated with a series of depolarising voltage pulses (the time from the start of the experiment is indicated in the top of the panels and the voltage at the bottom). The upper panel shows the R-GECO1 signal, while the lower panels display the magnified images, as indicated by the white dashed line. The transmitted light image of this cell is shown in the lower right panel. The calibration bar (upper right) links the colour code to the fluorescence intensity of R-GECO1. (b, c) *Top panels*: voltage protocols to stimulate cells either with a series of depolarising (b) or hyperpolarising (c) pulses. *Middle panels*: averaged values of the R-GECO1 fluorescence intensity (normalised to the value at the start of the experiment, black) at the region of interest (ROI, as indicated in upper panel of (a)), as well as the calculated pH-dependent changes in R-GECO1 fluorescence, deduced from cpYFP-recordings (grey). *Bottom panels*: Average  $\text{Ca}^{2+}$ -dependent R-GECO1 signal calculated by subtracting the pH-dependent signal (grey, middle panel) from the total R-GECO1 signal (black, middle panel). The solid straight lines represent the slope of the initial  $[\text{Ca}^{2+}]_{\text{cyt}}$ -dependent R-GECO1 fluorescence change, in response to a voltage change. Error bars show SE ( $n = 7$ ). (d) The average rates of R-GECO1 initial fluorescence changes (black straight lines in (b) and (c), lower panels) are plotted against the applied voltage. The solid black lines show linear fits, with the indicated correlation coefficients. Error bars show SE ( $n = 7$ ).

### Are VM-dependent $[\text{Ca}^{2+}]_{\text{cyt}}$ changes caused by $\text{H}^+/\text{Ca}^{2+}$ exchangers?

Changes in the  $[\text{Ca}^{2+}]_{\text{cyt}}$  of plant cells are often accompanied by pH changes in the same compartment (Behera *et al.*, 2018; Waadt *et al.*, 2020). We therefore used seedlings that expressed cpYFP to monitor the cytosolic pH during manipulation of the VM (Fig. 3). It turned out that depolarisation of the VM in steps of 30 s caused an alkalinisation of the cytosol (Fig. 3a,b), whereas hyperpolarising pulses provoked acidification (Fig. 3a,c). The potential of the VM membrane, therefore, appears to affect both the cytosolic pH (Fig. 3d) and  $\text{Ca}^{2+}$  concentration.

We set out to elucidate the nature of the transporter that provokes the changes in  $[\text{Ca}^{2+}]_{\text{cyt}}$  upon manipulation of the

VM potential. To this purpose, the relationship between  $[\text{Ca}^{2+}]_{\text{cyt}}$  and the VM was determined with voltage pulses ranging from +100 mV to +20 mV (Fig. 4a,b), as well as pulses ranging from -80 mV to -20 mV (Fig. 4c). In this respect, we had to overcome the technical difficulty that the fluorescence intensity of R-GECO1 is sensitive to changes in  $[\text{Ca}^{2+}]_{\text{cyt}}$ , as well as the cytosolic pH (Zhao *et al.* 2011). We therefore developed a procedure, to determine the impact of cytosolic pH changes on R-GECO1, using the cpYFP signal as a reference. This approach revealed that the voltage-induced cytosolic pH changes only had a small impact on R-GECO1 (Fig. 4d) and therefore that most of the changes in the R-GECO1 signal during the voltage pulses are due to a change in  $[\text{Ca}^{2+}]_{\text{cyt}}$  (Fig. 4b-d).

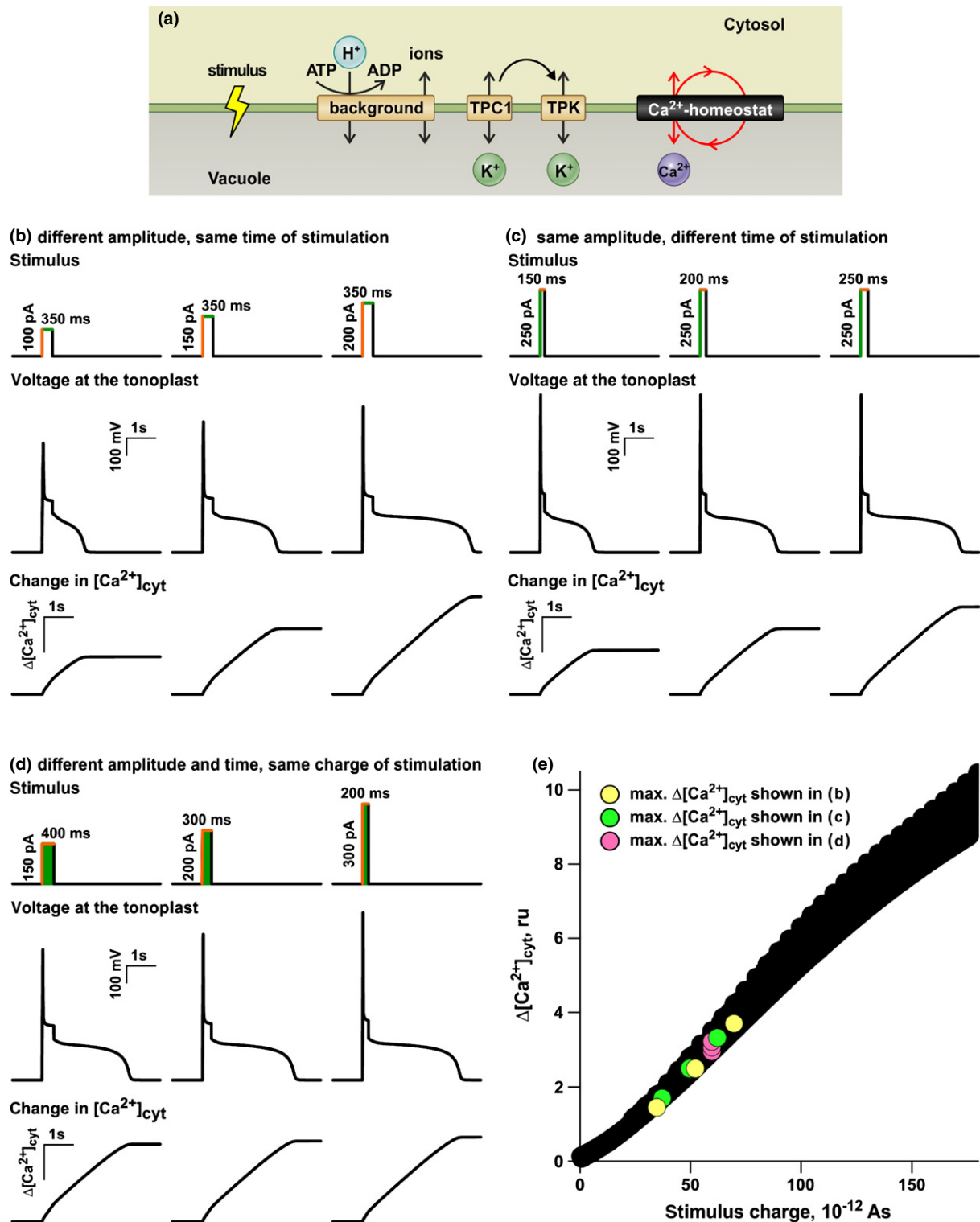


**Fig. 5** Theoretical thermodynamic characteristics of potential  $\text{Ca}^{2+}$  transporters in the vacuolar membrane (VM). (a–d) Change in Gibbs free energy plotted against the potential of the VM of a  $\text{H}^+/\text{Ca}^{2+}$  exchange mechanism with  $\text{H}^+/\text{Ca}^{2+}$  transport stoichiometries of 4 : 1 (a), 3 : 1 (b), 2 : 1 (c) and 1 : 1 (d) for a transmembrane pH gradient (luminal more acidic) of 1 (black), 1.5 (magenta) and 2 (cyan) units. The  $\text{Ca}^{2+}$  gradient was set at  $[\text{Ca}^{2+}]_{\text{lum}}/[\text{Ca}^{2+}]_{\text{cyt}} = 10^4$ . (e) Change in Gibbs free energy plotted against the potential of the VM of a  $\text{Ca}^{2+}$  permeable ion channel operating under luminal/cytosolic  $\text{Ca}^{2+}$  gradients of  $10^3$  (magenta) and  $10^4$  (black). (f) Change in Gibbs free energy plotted against the potential of the VM of a  $\text{Ca}^{2+}$ -ATPase mechanism exchanging 2  $\text{Ca}^{2+}$  ions for 2 protons (Yu *et al.*, 1993; Olesen *et al.*, 2007) that operates under a luminal/cytosolic  $\text{Ca}^{2+}$  gradient of  $10^4$  and transmembrane pH gradients (luminal more acidic) of 1 (black), 1.5 (magenta) and 2 (cyan) units. For  $\Delta G > 0$  the driving force for the  $\text{Ca}^{2+}$  flux would be from the lumen to the cytosol and for  $\Delta G < 0$  the driving force would be from the cytosol to the lumen. Note that the only mechanism that mediates a  $\text{Ca}^{2+}$  influx upon depolarisation and a  $\text{Ca}^{2+}$  efflux upon hyperpolarisation under physiological conditions is a  $m\text{H}^+/n\text{Ca}^{2+}$  exchange with  $m/n > 2$  (a, b).

The relationship between changes in the VM potential ( $\Delta V_{\text{T}} = \psi_{\text{bath}} - \Delta\psi_{\text{vac}}$ ) and the rate by which the  $\text{Ca}^{2+}$ -dependent R-GECO1 signal changed is shown in Fig. 4(b,c). Both the

data obtained at depolarising and hyperpolarising pulses were fitted with a linear function, which revealed an  $r^2$  of 0.99 and 0.75, respectively. If we assume that the change in the R-GECO1





**Fig. 6** Impact of vacuolar membrane (VM) excitation by the TPC1/TPK module on Ca<sup>2+</sup><sub>cyt</sub> control by the Ca<sup>2+</sup> homeostat. (a) Schematic representation of the transporters of the vacuolar excitation module (H<sup>+</sup>-ATPase-dominated background current, the TPC1 and TPK channels) together with the Ca<sup>2+</sup> homeostat. An external stimulus can excite the tonoplast, which then affects the Ca<sup>2+</sup> homeostat and alters the cytosolic Ca<sup>2+</sup> concentration. (b) Current stimuli of varying amplitude excite the VM in a stimulus-dependent manner and provoke a stimulus-dependent release of Ca<sup>2+</sup> to the cytosol. (c) Current stimuli of varying duration excite the VM in a stimulus-dependent manner and provoke a stimulus-dependent release of Ca<sup>2+</sup> to the cytosol. (d) If stimulus amplitude and duration are varied in a way that the total charge of the stimulus (green area) is constant, the VM becomes excited to a similar degree and the magnitude of Ca<sup>2+</sup> current from the vacuole to the cytosol is the same. (e) Relationship between stimulus charge and rise in [Ca<sup>2+</sup>]<sub>cyt</sub>; 818 different conditions have been simulated. Each black dot represents a tested condition. The coloured dots indicate the final Δ[Ca<sup>2+</sup>]<sub>cyt</sub> for the cases presented in b (yellow), c (green) and d (pink).

signal is a measure of the  $\text{Ca}^{2+}$  current across the VM, this  $\text{Ca}^{2+}$  current, therefore, has a linear dependency on the VM potential (Fig. 4d). The  $\text{Ca}^{2+}$  conductance of the VM was compared with that of several groups of  $\text{Ca}^{2+}$  transporters (Fig. 5). Among the possibilities tested, we found that an  $\text{mH}^+/\text{nCa}^{2+}$  exchanger with a coupling rate  $m/n > 2$  provided the best fit of our experimental observations (compare Fig. 5a,b with Fig. 4d). By contrast,  $\text{mH}^+/\text{nCa}^{2+}$  exchangers with a coupling rate of  $m/n$  less than 2 (Fig. 5c,d), ion channels (Fig. 5e), or  $\text{Ca}^{2+}$ -ATPases (Fig. 5f) showed a thermodynamic behaviour that clearly deviated from that of the  $\text{Ca}^{2+}$  current across the VM. We therefore regard it unlikely that the latter groups of  $\text{Ca}^{2+}$  transport proteins contributed essentially to the measured voltage-dependent VM  $\text{Ca}^{2+}$  conductance.

Altogether, our data suggested the presence of active  $\text{H}^+/\text{Ca}^{2+}$  exchangers in the VM. A depolarisation of the VM reduced the driving force for the  $\text{H}^+$  flux into the cytosol and as a result caused an increase in pH (Fig. 3). The lowered driving force of  $\text{H}^+$  also reduced the uptake of  $\text{Ca}^{2+}$  by  $\text{H}^+/\text{Ca}^{2+}$  exchangers into the vacuole and therefore caused a rise in  $[\text{Ca}^{2+}]_{\text{cyt}}$  (Fig. 4). An inverse behaviour was observed upon hyperpolarisation. The CAX genes are obvious candidates to encode these voltage-dependent VM-localised transporters, as most CAX transporters are located in the vacuole and act as  $\text{H}^+/\text{Ca}^{2+}$  exchangers (Pittman & Hirschi, 2016). Future studies will have to reveal if CAX-proteins indeed serve as voltage-dependent vacuolar  $\text{Ca}^{2+}$  homeostats, or if other metal transporters also contribute to this system that balances  $[\text{Ca}^{2+}]_{\text{cyt}}$ .

### A model that couples VM excitation to $[\text{Ca}^{2+}]_{\text{cyt}}$ signals

The physiological function of the voltage-dependent  $\text{Ca}^{2+}$  conductance of the VM (called  $\text{Ca}^{2+}$  homeostat in the following) was explored using computer-based simulations. Recently, it was shown that the voltage-dependent channel TPC1 and the  $\text{K}^+$  selective channels TPK1/TPK3 can convert an initial short voltage stimulus into a prolonged depolarisation of the VM (Jaslan *et al.*, 2019). This experimentally observed mechanism was simulated with high accuracy by a computational model (Jaslan *et al.*, 2019) that was now expanded with the VM-based  $\text{Ca}^{2+}$  homeostat (Fig. 6a).

As demonstrated by Jaslan *et al.* (2019) the application of a current pulse depolarised the VM and the length of the depolarisation depended on the strength of the current pulse (Fig. 6b). During the depolarisation,  $\text{Ca}^{2+}_{\text{cyt}}$  increased and stronger current pulses enhanced this response. Likewise, the magnitude of the  $[\text{Ca}^{2+}]_{\text{cyt}}$  change was enhanced, if the length of the current pulses was increased (Fig. 6c). However, when both amplitude and time were varied, but the stimulus charge (product of current and time) was kept constant, both the excitation time and final level of  $[\text{Ca}^{2+}]_{\text{cyt}}$  remained unchanged (Fig. 6d). We screened the  $[\text{Ca}^{2+}]_{\text{cyt}}$  vs charge relationship for a huge set of time/amplitude-combinations (black dots in Fig. 6e) and found an unambiguous relationship between the calcium signals and the stimulus charge. Therefore, the VM seems capable of integrating the amplitude and length of current pulses and convert these parameters into a

voltage change, which in turn provokes a cytosolic  $\text{Ca}^{2+}$  signal (Fig. 6e).

The combined  $\text{Ca}^{2+}$  homeostat and the TPC1/TPK1/TPK3-based channel network in the VM may, therefore, explain how the voltage-dependent TPC1 cation channels, together with the  $\text{Ca}^{2+}$ -dependent  $\text{K}^+$  channels TPK1 and TPK3, contribute to shaping the  $\text{Ca}^{2+}$  signals, while none of these channels directly releases  $\text{Ca}^{2+}$  from the vacuole. The proposed  $\text{Ca}^{2+}$ -release model is in line with the observed role of TPC1 in long distance signals, which are provoked by high NaCl concentrations in roots (Choi *et al.*, 2014) and herbivory in shoots (Kiep *et al.*, 2015). It is likely that these  $\text{Ca}^{2+}$  signals are passed on from one cell to its neighbour by plasmodesmata (Hedrich *et al.*, 2016; Choi *et al.*, 2017). Because of these connections, elevation of  $\text{Ca}^{2+}_{\text{cyt}}$  in a certain cell may cause a small local  $\text{Ca}^{2+}$  signal in the neighbouring cell. In return, the localised  $\text{Ca}^{2+}$  signal in the neighbour cell can activate TPK channels by the  $\text{Ca}^{2+}$ -binding calcineurin B-like (CBL) proteins that regulate CBL-interacting protein kinases (Gobert *et al.*, 2007; Latz *et al.*, 2007; Voelker *et al.*, 2010; Wang *et al.*, 2015; Tang *et al.*, 2020), depolarise the VM and trigger a large rise in  $[\text{Ca}^{2+}]_{\text{cyt}}$  through the  $\text{Ca}^{2+}$  homeostat of the VM.




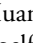
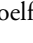
### Acknowledgements

The authors are grateful to Rainer Waadt (University of Tartu, Estonia), Melanie Krebs and Karin Schumacher (University of Heidelberg, Germany), for providing the Arabidopsis lines expressing R-GECO1 and GFP5, while the cpYFP expressing line was a generous gift from Markus Schwarzländer (University of Münster, Germany). This work was funded by grants from the Deutsche Forschungsgemeinschaft to MRGR (GK 1342, Project B5; RO2381/8-1), a DFG Koselleck award to RH (HE1640/42-1), a postdoctoral fellowship from the European Molecular Biology Organization to JD (EMBO ALTF 683-2018), the China Scholarship Council (CSC) to SH (201506350031) and the Fondo para Proyectos de Investigación Enlace Fondecyt of the Universidad Talca to ID.

### Author contributions

JD, MRGR, SH and RH designed the wet laboratory experiments. JD and SH conducted and analysed electrophysiological and imaging experiments. JD modelled the transporter thermodynamics. ID designed and conducted mathematical modelling. All authors contributed to writing of the manuscript. JD and ID contributed equally to this work.

### ORCID

Julian Dindas  <https://orcid.org/0000-0003-3078-4865>  
 Ingo Dreyer  <https://orcid.org/0000-0002-2781-0359>  
 Rainer Hedrich  <https://orcid.org/0000-0003-3224-1362>  
 Shouguang Huang  <https://orcid.org/0000-0001-7007-0301>  
 M. Rob G. Roelfsema  <https://orcid.org/0000-0002-4076-4246>

## References

- Behera S, Xu ZL, Luoni L, Bonza MC, Doccula FG, De Michelis MI, Morris RJ, Schwarzlander M, Costa A. 2018. Cellular  $\text{Ca}^{2+}$  signals generate defined pH signatures in plants. *Plant Cell* 30: 2704–2719.
- Bertl A, Blumwald E, Coronado R, Eisenberg R, Findlay G, Gradmann D, Hille B, Kohler K, Kolb HA, Macrobbe E *et al.* 1992. Electrical measurements on endomembranes. *Science* 258: 873–874.
- Bethmann B, Thaler M, Simonis W, Schonknecht G. 1995. Electrochemical potential gradients of  $\text{H}^+$ ,  $\text{K}^+$ ,  $\text{Ca}^{2+}$ , and  $\text{Cl}^-$  across the tonoplast of the green alga *Eremosphaera viridis*. *Plant Physiology* 109: 1317–1326.
- Bose J, Pottosin II, Shabala SS, Palmgren MG, Shabala S. 2011. Calcium efflux systems in stress signaling and adaptation in plants. *Frontiers in Plant Science* 2: 17.
- Choi WG, Miller G, Wallace I, Harper J, Mittler R, Gilroy S. 2017. Orchestrating rapid long-distance signaling in plants with  $\text{Ca}^{2+}$ , ROS and electrical signals. *The Plant Journal* 90: 698–707.
- Choi WG, Toyota M, Kim SH, Hilleary R, Gilroy S. 2014. Salt stress-induced  $\text{Ca}^{2+}$  waves are associated with rapid, long-distance root-to-shoot signaling in plants. *Proceedings of the National Academy of Sciences, USA* 111: 6497–6502.
- Costa A, Luoni L, Marrano CA, Hashimoto K, Koster P, Giacometti S, De Michelis MI, Kudla J, Bonza MC. 2017.  $\text{Ca}^{2+}$ -dependent phosphoregulation of the plasma membrane  $\text{Ca}^{2+}$ -ATPase ACA8 modulates stimulus-induced calcium signatures. *Journal of Experimental Botany* 68: 3215–3230.
- Dempster J. 1997. A new version of the Strathclyde Electrophysiology software package running within the Microsoft Windows environment. *Journal of Physiology-London* 504P: P57.
- Dindas J, Scherzer S, Roelfsema MRG, von Meyer K, Muller HM, Al-Rasheid KAS, Palme K, Dietrich P, Becker D, Bennett MJ *et al.* 2018. AUX1-mediated root hair auxin influx governs SCFTIR1/AFB-type  $\text{Ca}^{2+}$  signaling. *Nature Communications* 9: 10.
- Evans MJ, Choi WG, Gilroy S, Morris RJ. 2016. A ROS-assisted calcium wave dependent on the ARBOHD NADPH oxidase and TPC1 cation channel propagates the systemic response to salt stress. *Plant Physiology* 171: 1771–1784.
- Felle H. 1988. Cytoplasmic free calcium in *Riccia fluitans* l and *Zea mays* - interaction of  $\text{Ca}^{2+}$  and pH. *Planta* 176: 248–255.
- Frietsch S, Wang YF, Sladek C, Poulsen LR, Romanowsky SM, Schroeder JI, Harper JF. 2007. A cyclic nucleotide-gated channel is essential for polarized tip growth of pollen. *Proceedings of the National Academy of Sciences, USA* 104: 14531–14536.
- Gobert A, Isayenkov S, Voelker C, Czempinski K, Maathuis FJM. 2007. The two-pore channel *TPK1* gene encodes the vacuolar  $\text{K}^+$  conductance and plays a role in  $\text{K}^+$  homeostasis. *Proceedings of the National Academy of Sciences, USA* 104: 10726–10731.
- Grabov A, Blatt MR. 1998. Membrane voltage initiates  $\text{Ca}^{2+}$  waves and potentiates  $\text{Ca}^{2+}$  increases with abscisic acid in stomatal guard cells. *Proceedings of the National Academy of Sciences, USA* 95: 4778–4783.
- Hamilton DWA, Hills A, Kohler B, Blatt MR. 2000.  $\text{Ca}^{2+}$  channels at the plasma membrane of stomatal guard cells are activated by hyperpolarization and abscisic acid. *Proceedings of the National Academy of Sciences, USA* 97: 4967–4972.
- Hamilton ES, Schlegel AM, Haswell ES. 2015. United in diversity: Mechanosensitive ion channels in plants. *Annual Review of Plant Biology* 66: 113–137.
- Hedrich R, Mueller TD, Becker D, Marten I. 2018. Structure and function of TPC1 vacuole SV channel gains shape. *Molecular Plant* 11: 764–775.
- Hedrich R, Salvador-Recatala V, Dreyer I. 2016. Electrical wiring and long-distance plant communication. *Trends in Plant Science* 21: 376–387.
- Heim R, Cubitt AB, Tsien RY. 1995. Improved green fluorescence. *Nature* 373: 663–664.
- Hou CC, Tian W, Kleist T, He K, Garcia V, Bai FL, Hao YL, Luan S, Li LG. 2014. DUF221 proteins are a family of osmosensitive calcium-permeable cation channels conserved across eukaryotes. *Cell Research* 24: 632–635.
- Huang SG, Waadt R, Nuhkat M, Kollist H, Hedrich R, Roelfsema MRG. 2019. Calcium signals in guard cells enhance the efficiency by which abscisic acid triggers stomatal closure. *New Phytologist* 224: 177–187.
- Isayenkov S, Isner JC, Maathuis FJM. 2010. Vacuolar ion channels: roles in plant nutrition and signalling. *FEBS Letters* 584: 1982–1988.
- Jaslan D, Dreyer I, Lu JP, O'Malley R, Dindas J, Marten I, Hedrich R. 2019. Voltage-dependent gating of SV channel TPC1 confers vacuole excitability. *Nature Communications* 10: 9.
- Jeworutzki E, Roelfsema MRG, Anschutz U, Krol E, Elzenga JTM, Felix G, Boller T, Hedrich R, Becker D. 2010. Early signaling through the *Arabidopsis* pattern recognition receptors FLS2 and EFR involves  $\text{Ca}^{2+}$ -associated opening of plasma membrane anion channels. *The Plant Journal* 62: 367–378.
- Keinath NF, Waadt R, Brugman R, Schroeder JI, Grossmann G, Schumacher K, Krebs M. 2015. Live cell imaging with R-GECO1 sheds light on flg22- and chitin-induced transient  $\text{Ca}^{2+}$  (cyt) patterns in *Arabidopsis*. *Molecular Plant* 8: 1188–1200.
- Kiep V, Vadassery J, Latke J, Maass JP, Boland W, Peiter E, Mithofer A. 2015. Systemic cytosolic  $\text{Ca}^{2+}$  elevation is activated upon wounding and herbivory in *Arabidopsis*. *New Phytologist* 207: 996–1004.
- Kudla J, Becker D, Grill E, Hedrich R, Hippler M, Kummer U, Parniske M, Romeis T, Schumacher K. 2018. Advances and current challenges in calcium signaling. *New Phytologist* 218: 414–431.
- Kurusu T, Kuchitsu K, Nakano M, Nakayama Y, Iida H. 2013. Plant mechanosensing and  $\text{Ca}^{2+}$  transport. *Trends in Plant Science* 18: 227–233.
- Latz A, Becker D, Hekman M, Muller T, Beyhl D, Marten I, Eing C, Bihler H, Fischer A, Dunkel M *et al.* 2007. TPK1, a  $\text{Ca}^{2+}$ -regulated *Arabidopsis* vacuole two-pore  $\text{K}^+$  channel is activated by 14-3-3 proteins. *The Plant Journal* 55: 449–459.
- Levchenko V, Konrad KR, Dietrich P, Roelfsema MRG, Hedrich R. 2005. Cytosolic abscisic acid activates guard cell anion channels without preceding  $\text{Ca}^{2+}$  signals. *Proceedings of the National Academy of Sciences, USA* 102: 4203–4208.
- Li YW, Hu YF, Wang JW, Liu X, Zhang W, Sun LF. 2020. Structural insights into a plant mechanosensitive ion channel MSL1. *Cell Reports* 30: 4518–4527.
- Marhavy P, Kurenda A, Siddique S, Tendon VD, Zhou F, Holbein J, Hasan MS, Grundler FMW, Farmer EE, Geldner N. 2019. Single-cell damage elicits regional, nematode-restricting ethylene responses in roots. *EMBO Journal* 38: 18.
- Martinoia E, Meyer S, De Angeli A, Nagy R. 2012. Vacuolar transporters in their physiological context. *Annual Review of Plant Biology* 63: 183–213.
- McAinsh MR, Pittman JK. 2009. Shaping the calcium signature. *New Phytologist* 181: 275–294.
- Michard E, Lima PT, Borges F, Silva AC, Portes MT, Carvalho JE, Gilliam M, Liu LH, Obermeyer G, Feijo JA. 2011. Glutamate receptor-like genes form  $\text{Ca}^{2+}$  channels in pollen tubes and are regulated by pistil D-serine. *Science* 332: 434–437.
- Miller AJ, Sanders D. 1987. Depletion of cytosolic free calcium induced by photosynthesis. *Nature* 326: 397–400.
- Mousavi SAR, Dubin AE, Zeng W-Z, Do K, Ghadir DA, Ge C, Zhao Y, Patapoutian A. 2020. PIEZO ion channel is required for root mechanotransduction in *Arabidopsis thaliana*. *BioRxiv*. 10.1101/2020.08.27.270355
- Nguyen CT, Kurenda A, Stolz S, Chetelat A, Farmer EE. 2018. Identification of cell populations necessary for leaf-to-leaf electrical signaling in a wounded plant. *Proceedings of the National Academy of Sciences, USA* 115: 10178–10183.
- Olesen C, Picard M, Winther AML, Gyrop C, Morth JP, Oxvig C, Moller JV, Nissen P. 2007. The structural basis of calcium transport by the calcium pump. *Nature* 450: 1036–1042.
- Pan YJ, Chai XY, Gao QF, Zhou LM, Zhang SS, Li LG, Luan S. 2019. Dynamic interactions of plant CNGC subunits and calmodulins drive oscillatory  $\text{Ca}^{2+}$  channel activities. *Developmental Cell* 48: 710–725.
- Pei ZM, Murata Y, Benning G, Thomine S, Klusener B, Allen GJ, Grill E, Schroeder JI. 2000. Calcium channels activated by hydrogen peroxide mediate abscisic acid signalling in guard cells. *Nature* 406: 731–734.
- Peiter E, Maathuis FJM, Mills LN, Knight H, Pelloux J, Hetherington AM, Sanders D. 2005. The vacuolar  $\text{Ca}^{2+}$ -activated channel TPC1 regulates germination and stomatal movement. *Nature* 434: 404–408.
- Pittman JK, Hirschi KD. 2016. CAX-ing a wide net: cation/ $\text{H}^+$  transporters in metal remediation and abiotic stress signalling. *Plant Biology* 18: 741–749.

- Pratt J, Boisson AM, Gout E, Bligny R, Douce R, Aubert S. 2009. Phosphate (Pi) starvation effect on the cytosolic Pi concentration and Pi exchanges across the tonoplast in plant cells: An *in vivo* P-31-nuclear magnetic resonance study using methylphosphonate as a Pi analog. *Plant Physiology* 151: 1646–1657.
- Radin I, Richardson RA, Weiner ER, Bascom CS, Bezanilla M, Haswell ES. 2020. Regulation of vacuole morphology by Piezo channels in spreading earth moss. *BioRxiv*. 10.1101/2020.08.27.269282.
- Ranf S, Eschen-Lippold L, Frhlich K, Westphal L, Scheel D, Lee J. 2014. Microbe-associated molecular pattern-induced calcium signaling requires the receptor-like cytoplasmic kinases, PBL1 and BIK1. *BMC Plant Biology* 14: Article Nr. 374.
- Roelfsema MRG, Hedrich R. 2010. Making sense out of Ca<sup>2+</sup> signals: their role in regulating stomatal movements. *Plant, Cell & Environment* 33: 305–321.
- Schindelin J, Arganda-Carreras I, Frise E, Kaynig V, Longair M, Pietzsch T, Preibisch S, Rueden C, Saalfeld S, Schmid B *et al.* 2012. Fiji: an open-source platform for biological-image analysis. *Nature Methods* 9: 676–682.
- Schwarzländer M, Logan DC, Fricker MD, Sweetlove LJ. 2011. The circularly permuted yellow fluorescent protein cpYFP that has been used as a superoxide probe is highly responsive to pH but not superoxide in mitochondria: implications for the existence of superoxide 'flashes'. *Biochemical Journal* 437: 381–387.
- Shih HW, DePew CL, Miller ND, Monshausen GB. 2015. The cyclic nucleotide-gated channel CNGC14 regulates root gravitropism in *Arabidopsis thaliana*. *Current Biology* 25: 3119–3125.
- Siemering KR, Golbik R, Sever R, Haseloff J. 1996. Mutations that suppress the thermosensitivity of green fluorescent protein. *Current Biology* 6: 1653–1663.
- Stange A, Hedrich R, Roelfsema MRG. 2010. Ca<sup>2+</sup>-dependent activation of guard cell anion channels, triggered by hyperpolarization, is promoted by prolonged depolarization. *The Plant Journal* 62: 265–276.
- Stoelzle S, Kagawa T, Wada M, Hedrich R, Dietrich P. 2003. Blue light activates calcium-permeable channels in *Arabidopsis* mesophyll cells via the phototropin signaling pathway. *Proceedings of the National Academy of Sciences, USA* 100: 1456–1461.
- Tang RJ, Luan S. 2017. Regulation of calcium and magnesium homeostasis in plants: from transporters to signaling network. *Current Opinion in Plant Biology* 39: 97–105.
- Tang RJ, Zhao F-G, Yang Y, Wang C, Li K, Kleist TJ, Lemaux PG, Luan S. 2020. A calcium signalling network activates vacuolar K<sup>+</sup> remobilization to enable plant adaptation to low-K environments. *Nature Plants*. 6: 384–393.
- Thor K, Jiang SS, Michard E, George J, Scherzer S, Huang SG, Dindas J, Derbyshire P, Leitao N, DeFalco TA *et al.* 2020. The calcium-permeable channel OSCA1.3 regulates plant stomatal immunity. *Nature* 585: 569–573.
- Tian W, Hou CC, Ren ZJ, Wang C, Zhao FG, Dahlbeck D, Hu SP, Zhang LY, Niu Q, Li LG *et al.* 2019. A calmodulin-gated calcium channel links pathogen patterns to plant immunity. *Nature* 572: 131–135.
- Toyota M, Spencer D, Sawai-Toyota S, Wang JQ, Zhang T, Koo AJ, Howe GA, Gilroy S. 2018. Glutamate triggers long-distance, calcium-based plant defense signaling. *Science* 361: 1112–1115.
- Trewavas A. 1999. Le calcium, C'est la vie: calcium makes waves. *Plant Physiology* 120: 1–6.
- Tunc-Ozdemir M, Rato C, Brown E, Rogers S, Mooneyham A, Frietsch S, Myers CT, Poulsen LR, Malho R, Harper JF. 2013. Cyclic nucleotide gated channels 7 and 8 are essential for male reproductive fertility. *PLoS ONE* 8: 8.
- Voelker C, Gomez-Porras JL, Becker D, Hamamoto S, Uozumi N, Gambale F, Mueller-Roeber B, Czempinski K, Dreyer I. 2010. Roles of tandem-pore K<sup>+</sup> channels in plants – a puzzle still to be solved. *Plant Biology* 12: 56–63.
- Voss LJ, Hedrich R, Roelfsema MRG. 2016. Current injection provokes rapid expansion of the guard cell cytosolic volume and triggers Ca<sup>2+</sup> signals. *Molecular Plant* 9: 471–480.
- Waadt R, Koster P, Andres Z, Waadt C, Bradamante G, Lampou K, Kudla J, Schumacher K. 2020. Dual-reporting transcriptionally linked genetically encoded fluorescent indicators resolve the spatiotemporal coordination of cytosolic abscisic acid and second messenger dynamics in *Arabidopsis*. *Plant Cell* 32: 2582–2601.
- Wang Y, Dindas J, Rienmuller F, Krebs M, Waadt R, Schumacher K, Wu W-H, Hedrich R, Roelfsema MRG. 2015. Cytosolic Ca<sup>2+</sup> signals enhance the vacuolar ion conductivity of bulging *Arabidopsis* root hair cells. *Molecular Plant* 8: 1665–1674.
- Wheeler GL, Brownlee C. 2008. Ca<sup>2+</sup> signalling in plants and green algae – changing channels. *Trends in Plant Science* 13: 506–514.
- Wudick MM, Portes MT, Michard E, Rosas-Santiago P, Lizzio MA, Nunes CO, Campos C, Daminieli DSC, Carvalho JC, Lima PT *et al.* 2018. CORNICHON sorting and regulation of GLR channels underlie pollen tube Ca<sup>2+</sup> homeostasis. *Science* 360: 533–536.
- Xu J, Li HD, Chen LQ, Wang Y, Liu LL, He L, Wu WH. 2006. A protein kinase, interacting with two calcineurin B-like proteins, regulates K<sup>+</sup> transporter AKT1 in *Arabidopsis*. *Cell* 125: 1347–1360.
- Yang DL, Shi ZY, Bao YM, Yan JP, Yang ZY, Yu HY, Li Y, Gou MY, Wang S, Zou BH *et al.* 2017. Calcium pumps and interacting BON1 protein modulate calcium signature, stomatal closure, and plant immunity. *Plant Physiology* 175: 424–437.
- Yu X, Carroll S, Rigaud JL, Inesi G. 1993. H<sup>+</sup> countertransport and electrogenicity of the sarcoplasmic-reticulum Ca<sup>2+</sup> pump in reconstituted proteoliposomes. *Biophysical Journal* 64: 1232–1242.
- Yuan F, Yang HM, Xue Y, Kong DD, Ye R, Li CJ, Zhang JY, Theprungsirikul L, Shrift T, Krichilsky B *et al.* 2014. OSCA1 mediates osmotic-stress-evoked Ca<sup>2+</sup> increases vital for osmosensing in *Arabidopsis*. *Nature* 514: 367–371.
- Zhao YX, Araki S, Jiahui WH, Teramoto T, Chang YF, Nakano M, Abdelfattah AS, Fujiwara M, Ishihara T, Nagai T *et al.* 2011. An expanded palette of genetically encoded Ca<sup>2+</sup> indicators. *Science* 333: 1888–1891.

## Supporting Information

Additional Supporting Information may be found online in the Supporting Information section at the end of the article.

**Fig. S1** Calibration of pH-induced changes of cpYFP and R-GECO1 fluorescence signals.

**Fig. S2** Cytosolic current pulses do not trigger Ca<sup>2+</sup> release at the PM.

Please note: Wiley Blackwell are not responsible for the content or functionality of any Supporting Information supplied by the authors. Any queries (other than missing material) should be directed to the *New Phytologist* Central Office.